Dynamic Susceptibility of Nanopillars

N. Dao[1], I. Dumitru[2], L. Spinu[2], S. L. Whittenburg[3], M. J. Donahue[4], and J. C. Lodder[1]

[1] Systems and Materials for Information Storage, MESA+ Institute, University of Twente, Enschede, the Netherlands
[2] Department of Physics/AMRI, University of New Orleans, New Orleans, Louisiana, USA
[3] Department of Chemistry/AMRI, University of New Orleans, New Orleans, Louisiana, USA
[4] National Institute of Standards and Technology, Gaithersburg, Maryland, USA

E-mail: n.dao@el.utwente.nl

Abstract

We have calculated dynamic susceptibility of patterned cobalt and Permalloy pillars with a diameter of 50 nm and different pillar heights using micromagnetic simulations. The resonance modes obtained from these simulations are compared to the results obtained from analytical solution of Kittel's equation for spheroids. We also compared directly to Kittel's equation with the simulation of cobalt spheroids.

1. Introduction

The rapid development of magnetic elements for data storage and MRAM devices with reduced dimensions has led to increased interest in dynamic properties of nanoshaped magnetic elements. Dynamic switching has been studied [1-4] and addressed the suppression of ringing [5-7]. With the aim of engineering high-speed magnetic devices, numerical calculations on different magnetic materials have also been reported [8-10]. Understanding spatial spin distribution in a particle also helps its dynamic reversal. Micromagnetic simulations can identify those non-homogeneous regions of spins. In this paper, we will discuss two theoretical calculations of the dynamic susceptibility in cobalt and Permalloy nanopillars.

2. Procedure

Three-dimensional Object-Oriented MicroMagnetic Framework (OOMMF) [11] was used for our calculations by solving the Landau-Lifshitz-Gilbert equation as a function of time:

$$\frac{dM}{dt} = -\gamma\, M \times H_{\text{eff}} + \frac{\alpha}{\mathrm{M}_s}\left(M \times \frac{dM}{dt} \right),$$

where:

$$H_{\text{eff}} = \frac{2\mathrm{K}_1}{\mu_o \mathrm{M}_s^{\,2}}(M \cdot \hat{u})\hat{u} + \frac{2\mathrm{A}}{\mu_o \mathrm{M}_s^{\,2}}\nabla^2 M - N \cdot M \quad . \qquad (1)$$

γ of $2.21\text{x}10^5$ m/A·s is the Gilbert gyromagnetic ratio. The damping constant, α, was 0.015, which is less than 0.2 for a dynamic study [12]. The effective field, H_{eff}, (equation 1) includes anisotropy (the first term on the right-hand side), exchange (the second term), and self-magnetostatic (the last term) interactions. No thermal fluctuation field was added, so all of these calculations were performed at 0 K. $\hat{u}$ is the unit anisotropy axis. N is the demagnetizing tensor [13] and has been numerically addressed [14]. The anisotropy constants, K_1, of $4.5\text{x}10^5$ J/m^3 for cobalt [15] and of –500 J/m^3 for Permalloy ($\mathrm{Ni}_{80}\mathrm{Fe}_{20}$) [16] were used for these calculations, in which the [0 0 1] direction is the easy axis for cobalt and the hard axis for Permalloy. The exchange stiffness constants, A, were 30 pJ/m for cobalt and 13 pJ/m for Permalloy. These exchange constants were only approximate for cobalt and Permalloy, respectively. Saturation magnetizations, M_s, of $1.4\text{x}10^6$ A/m for cobalt and of $8.6\text{x}10^5$ A/m for Permalloy were also used. A cubic cell size of 5 nm was taken, which is approximately the same as the exchange length, $\sqrt{2\mathrm{A}/\mu_o \mathrm{M}_s^{\,2}}$, for each material.

A range of pillars with aspect ratios (height/width) from 1 to 20 was simulated via micromagnetics. The diameter was 50 nm. The equilibrium configuration for three sections of the pillar is shown in figure 1. After the

equilibrium magnetization was obtained, a small external pulse $H(t)=1000\exp(-10^9 t)$ ($t \geq 0$) was applied perpendicular to the long axis of the pillar (z-direction). Here, H(t) is in A/m and t is in seconds. The amplitude of the pulse field was small enough to remain in the linear response region. The corresponding $H(\omega)$ was obtained by using Fast Fourier Transform or analytically as $H(\omega)=1000/(10^9+2\pi i\omega)$. The imaginary part of susceptibility was computed by dividing the Fourier transform of the response ($M(\omega)$) by the Fourier transform of the excitation ($H(\omega)$).

The susceptibility was also calculated using Kittel's equation for elongated ellipsoids [17]. For a general ellipsoid, a homogeneous external magnetic field produces a homogeneous magnetization in the sample. The demagnetizing factor depends on the ratio of ellipsoidal axis, a, b, c. For a prolate spheroid, with $a = b$ and $c > a$, using the notation $q = c/a$ we have:

$$N_x = N_y \tag{2}$$

$$N_z = \frac{1}{q^2-1}\left[\frac{q}{\sqrt{q^2-1}}\ln\left(q+\sqrt{q^2-1}\right)-1\right] \tag{3}$$

and

$$N_x + N_y + N_z = 1. \tag{4}$$

For a uniformly magnetized sample, with magnetization M_z, the resonance frequency has the form:

$$\omega_r = \frac{\gamma}{2\pi}\left\{\left[H_0+(N_x-N_z)M_z\right]\left[H_0+(N_y-N_z)M_z\right]\right\}^{1/2} \tag{5}$$

where H_0 is the external static field. Inserting equation (2) into equation (5), we have:

$$\omega_r = \frac{\gamma}{2\pi}\left[H_0+(N_x-N_z)M_z\right] \tag{6}.$$

In the case when $q = 1$, $\omega_r = \gamma H_0/(2\pi)$ which is applicable to spheres and when $q \to \infty$, $\omega_r = \gamma(H_0 + M_z/2)/(2\pi)$ for infinite cylinders (pillars).

3. Results

The dynamic susceptibility obtained from the simulation is shown in figure 2 for cobalt and in figure 3 for Permalloy at two different aspect ratios, AS=3 and 6. For both aspect ratios, there are two resonance modes. One peak is due to the spins at the ends (bottom and top) of the pillars. The other mode is due to the spins in the middle of the pillar. The domain patterns shown in figure 1 can be used to understand this result. Near the end of the pillar, the self-magnetostatic field is large and opposes the exchange field (and for cobalt, the anisotropy field). This decreases the effective field near the ends, which reduces the resonance frequency in this region as compared to the middle of the pillar. This effect has been observed previously in simulations of rectangular stripes [9]. We can therefore identify the low frequency peak in figures 2 and 3 with the regions near the ends of the pillars.

The spins in the middle of the pillar have a majority of spins on all sides and the exchange interaction tends to align these spins. Also, the demagnetizing field (and anisotropy field for cobalt) tends to align the spins along the long axis of the pillar in this region, which is in the same direction. Therefore, the spins in this region are under a favourable effective field, giving high frequency response. The high frequency peak can be explained quite well by the theoretical predictions of Kittel's equation for prolate spheroids. In Kittel's equation (equation 6), H_0 is used to saturate spins in one direction, which is the characteristic of a single domain. In our simulations, there was no external applied field; however, there was intrinsic anisotropy field. We took the anisotropy field ($2K_1/\mu_0 M_s$ (A/m)) for cobalt and Permalloy, respectively, as the exchange for H_0 in Kittel's equation. Figure 4 displays the peak position of the high frequency mode from spins of the middle of a pillar along with the prediction from applying Kittel's equation (solid line). Clearly, the high frequency peak corresponds to the same trend as the results from Kittel's. The assignment of this high frequency mode in figures 2 and 3 should correspond to a single-domain like particle since the spins are aligned from the middle of the pillar.

The relative magnitudes of the low and high frequency peaks can be explained by the relative volumes of the end and central regions of the pillars. The extent of the end regions is determined primarily by the self-magnetostatic field at the pillar ends. This field doesn't depend significantly on the overall part geometry, and so the size of the end regions is relatively fixed irrespective of the length of the cylinder. Conversely, the volume of the central region grows with the length of the cylinder. Thus, we expect the magnitude of the high frequency peak to increase relative to the magnitude of the low frequency peak as the length of the cylinder is increased. Indeed, a comparison of the AS=3 and AS=6 traces in figures 2 and 3 reveals this effect.

For aspect ratios of AS=3 and 6 (see figures 2 and 3) as well as 4 and 10 (not shown), there appears additional fine structure in the high frequency peak. This fine structure is due to spin configuration the magnetization in the pillars as shown in figure 5. The convergence criterion in the simulation, a maximum torque for any spin of 0.12 deg/ns corresponding to a normalized torque of 10^{-5}, was the same for all aspect ratios and is quite conservative. The spin configuration is most likely not due to a lack of reaching an equilibrium structure prior to turning on the perturbing field. The spins in the region with this configuration are not as aligned as those in the middle region of the pillar and, therefore, have a slightly lower ferromagnetic resonance (FMR) frequency. The appearance of individual peaks (only two peaks for the AS of 6) in the fine structure could come from an artifact due to the discretization of the pillar into layers or due to an edge effect. Experimentally, the fine structure was also observed and due to magnetostatic waves since the magnetic field can be spatially inhomogeneous [18].

We can also examine the frequency for an infinite cylinder from Kittel's equation and compare with the value

of the frequency at the maximum aspect ratio obtained in the micromagnetic simulations. Using γ and saturation magnetizations of cobalt and Permalloy, Kittel's equation predicts 42.6 GHz for cobalt and 15.1 GHz for Permalloy, which agree well with the frequencies obtained from the micromagnetics simulation for the aspect ratio of 20 with 42.2 GHz for cobalt and 14.8 GHz for Permalloy. The difference between the results obtained from the simulation for an aspect ratio of 20 and an infinite cylinder from Kittel's equation is relatively the same for cobalt and Permalloy.

In order to get a better comparison between two calculation approaches, we also used a spheroid in the simulation. Figure 6, which displays the simulation as well as analytical Kittel's results for cobalt spheroids, shows that at higher aspect ratios, there is a nearly constant difference between the frequencies obtained from the simulation and those computed from Kittel's equation. This constant difference could be due to contributions from the surface effects. First, the spins near the surface are less free to rotate than the spins in the center of the spheroid, because the demagnetizing field attempts to align the spins parallel to the surface. Thus, we can envision a shell about the spheroid where the spins don't move as much. If the shell is of uniform thickness, then removing the shell yields a part with bigger aspect ratio. The remaining spins are those in the center of the spheroid, which have a greater freedom to rotate and, therefore, yield a lower frequency. An alternative explanation for the constant difference between the simulated frequencies and those obtained from Kittel's equation is discretization errors. The ideal spheroid has a smooth surface, but our computational cells are cubic, so the model has "stair-steps" on the surface. This is a limitation of the model. We have tested the magnitude of the discretization errors by simulating a cobalt spheroid with an aspect ratio of 2 with cell sizes of 2.5 nm x 2.5 nm x 2.5 nm and 1.67 nm x 1.67 nm x 2 nm. For both of these smaller cell sizes, the simulated frequency is 29.5 GHz compared to 29.1 GHz for the cell size of 5 nm. The frequency values for the smaller cell sizes are in closer agreement with Kittel's calculated value of 29.8 GHz, but not all of the difference can be explained in terms of discretization errors. It is possible to study a range of cell sizes, and extrapolate the frequencies obtained from the simulation to get a resonance frequency value, which is independent of discretization. However, the close agreement between the computed frequencies for the cobalt spheroid and the exact values from Kittel's equation is sufficient in this study.

4. Conclusions

By using a micromagnetic model together with the analytical method of Kittel's equation, we have shown that there are two major resonance modes in non-uniform magnetization structure. One mode represented the spins at the ends of a pillar, and the other mode was from the single-domain like spins. These characteristics have also been shown in rectangular Permalloy stripes [9]. The extension of this approach to calculation of multi-layer systems and to include consideration of thermal fluctuations and their affect on the precessional frequency would be an interesting subject for future study.

Acknowledgments

ND and JCL wish to acknowledge the support from Technology Foundation STW in the Netherlands (http://www.stw.nl/). SLW and LS acknowledge support of this work by the Louisiana Board of Regents and NSF via NSF/LEQSF(2001-04)-RII-03 and DARPA under MDA972-02-1-0012.

References

[1] A. Y. Elezzabi and M. R. Freeman 1996 Ultrafast magneto-optic sampling of picosecond current pulses *Appl. Phys. Lett.* **68** 3546.

[2] R. H. Koch, J. G. Deak, D. W. Abraham, P. L. Trouilloud, R. A. Altman, Yu Lu, W. J. Gallagher, R. E. Scheuerlein, K. P. Roche, and S. S. P. Parkin 1998 Magnetization reversal in micron-sized magnetic thin films *Phys. Rev. Lett.* **81** 4512.

[3] S. Kaka and S. Russek 2000 Switching in spin-valve devices in response to subnanosecond longitudinal field pulses *J. Appl. Phys.* **87** 6391.

[4] H. W. Schumacher, C. Chappert, R. C. Sousa, P. P. Freitas, and J. Miltat 2003 Quasiballistic magnetization reversal *Phys. Rev. Lett.* **90** 17204.

[5] M. Bauer, R. Lopusnik, J. Fassbender, and B. Hillebrands 2000 Suppression of magnetic field pulse-induced magnetization precession by pulse tailoring *Appl. Phys. Lett.* **76** 2758.

[6] Th. Gerrits, H. A. M. van den Berg, J. Hohlfeld, O. Gielkens, K. J. Veenstra, L. Bär, and Th. Rasing 2002 Picosecond precessional magnetization reversal by magnetic field pulse shaping *IEEE Trans. Magn.* **38** 2484.

[7] Th. Gerrits, H. A. M. van den Berg, J. Hohlfeld, L. Bär, and Th. Rasing 2002 Ultrafast precessional magnetization reversal by picosecond magnetic field pulse shaping *Nature* **418** 509.

[8] M. Bauer, J. Fassbender, and B. Hillebrands 2000 Switching behavior of a Stoner particle beyond the relaxation time limit *Phys. Rev. B* **61** 3410.

[9] O. Gérardin, H. Le Gall, M. J. Donahue, and N. Vukadinovic 2001 Micromagnetic calculation of the high frequency dynamics of nano-size rectangular ferromagnetic stripes *J. Appl. Phys.* **89** 7012.

[10] J. Fidler, T. Schrefl, V. D. Tsiantos, H. Forster, R. Dittrich, and D. Suess 2002 FE-Simulation of fast switching behavior of granular nanoelements *IEEE Trans. Magn.* **38** 2520.

[11] M. J. Donahue and D. Porter 1999 *Interagency Report **NISTIR 6376*** Gaithersburg (National Institute of Standards and Technology) (http://math.nist.gov/oommf).

[12] S. E. Russek, S. Kaka, and M. J. Donahue 2000 High Speed Dynamics, Damping, and Relaxation Times in Submicrometer Spin-Valve Devices *J. Appl. Phys.* **87** 7070.

[13] D. –X. Chen, J. A. Brug, and R. B. Goldfard 1991 Demagnetizing Factors for Cylinders *IEEE Trans. Magn.* **27** 3601.

[14] A. J. Newell, W. Williams, and D. J. Dunlop 1993 A Generalization of the Demagnetizing Tensor for Nonuniform Magnetization *J. Geophys. Res.* **98** 9551.

[15] R. M. Bozorth 1964 *Ferromagnetism* Princeton (D. Van Nostrand Company, Inc.) 568.

[16] R. A. McCurrie 1994 *Ferromagnetic Materials: Structure and Properties* San Diego (Academic Press) 29.

[17] C. Kittel 1948 On a theory of ferromagnetic resonance absorption *Phys. Rev*. **73** 155.

[18] S. E. Irvine and A. Y. Elezzabi 2003 Wideband Magneto-Optic Modulation in a Bismith-Substituted Yttrium Iron Garnet Waveguide *Opt. Comm.* **220** 325.

Figure captions

Figure 1. A flower state of cobalt pillar and a twisted flower state of Permalloy pillar, both with diameter of 50 nm and height of 150 nm. B stands for the spins at the bottom of a pillar, M for middle, and T for top in the x-y plane.

Figure 2. Imaginary susceptibility at two different aspect ratios (AS) for cobalt pillars.

Figure 3. Imaginary susceptibility at two different aspect ratios (AS) for Permalloy pillars.

Figure 4. Peak position of high-frequency modes of the dynamic susceptibility as obtained from the micromagnetics (cobalt (rectangular symbols) and Permalloy (circular symbols) pillars). The solid line is the prediction of Kittel's equation for a spheroid.

Figure 5. Spatial spins for a pillar with the aspect ratio of 6. The image on the left is for cobalt, and on the right for Permalloy. The spin configuration is in the equilibrium.

Figure 6. Simulation results (rectangular symbols) and Kittel's equation (solid line) for cobalt spheroids as a function of aspect ratio.

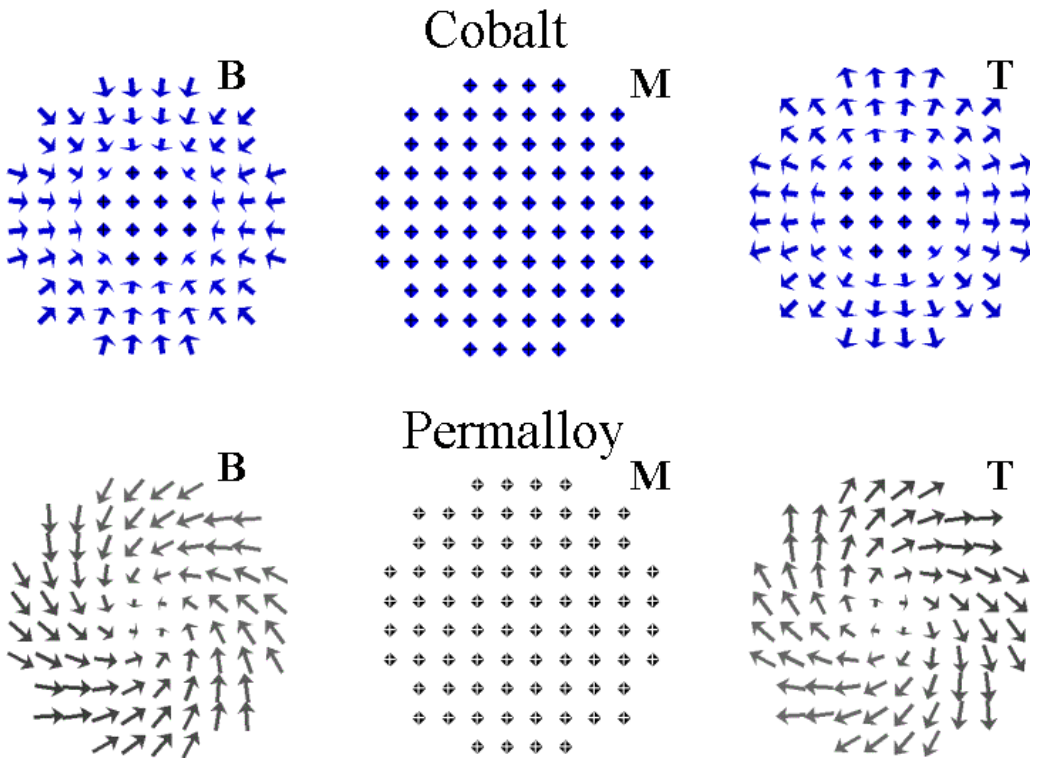

Figure 1
N. Dao, el al.

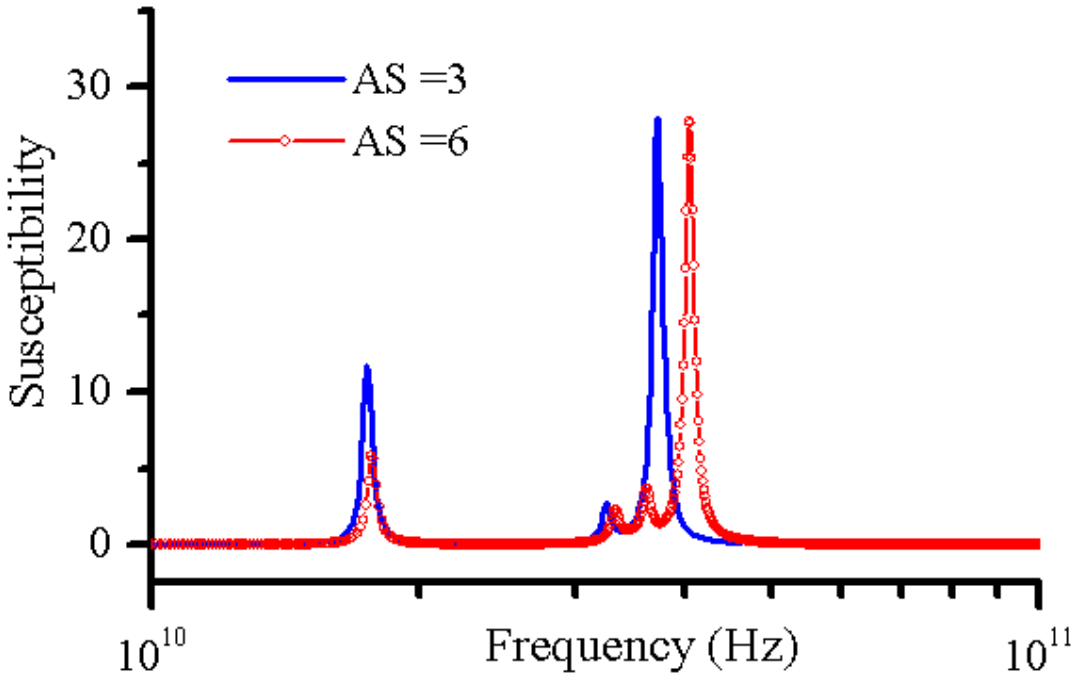

Figure 2
N. Dao, el al.

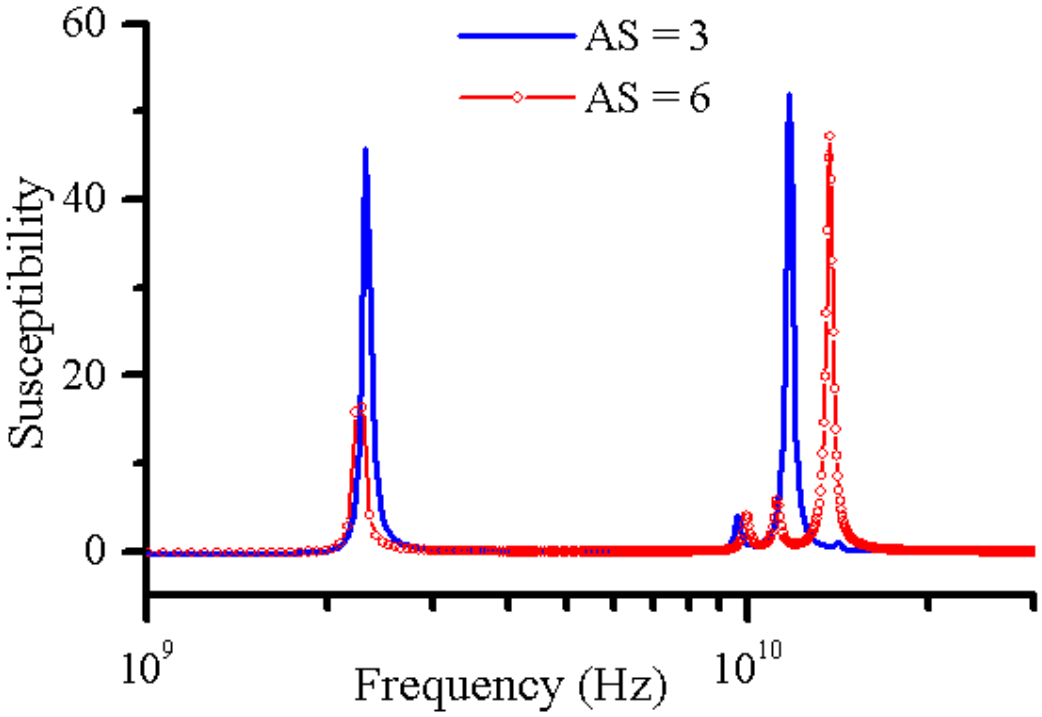

Figure 3
N. Dao, el al.

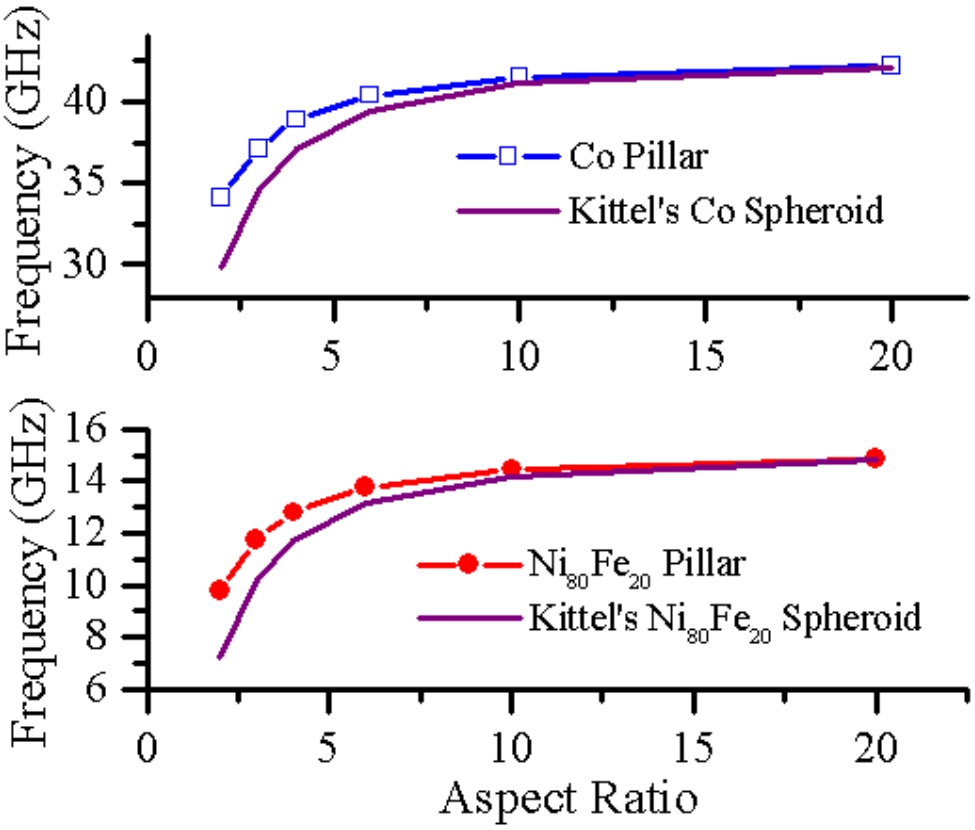

Figure 4
N. Dao, el al.

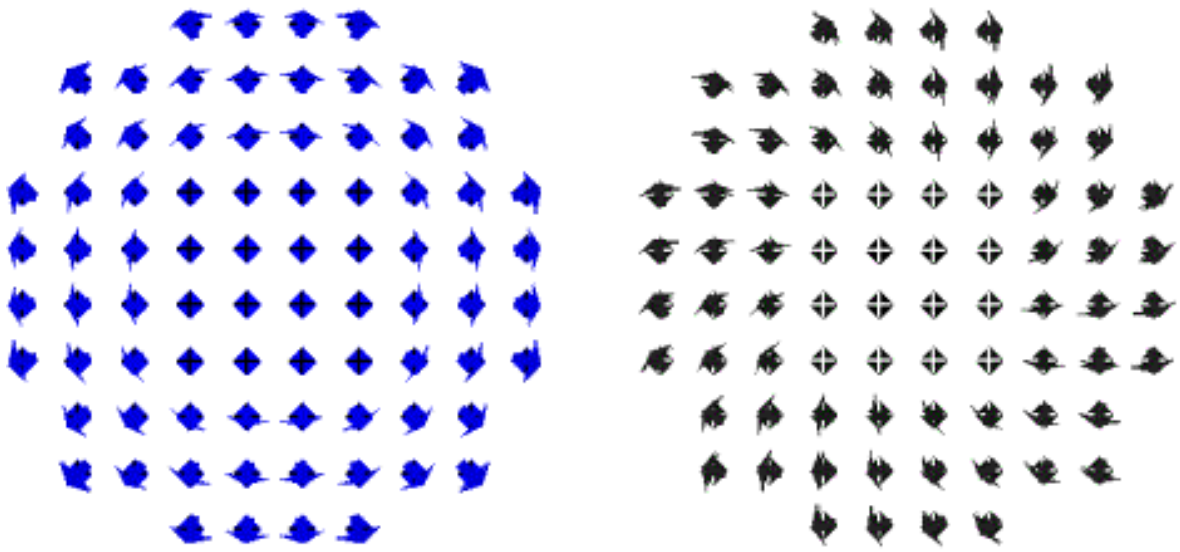

Figure 5
N. Dao, el al.

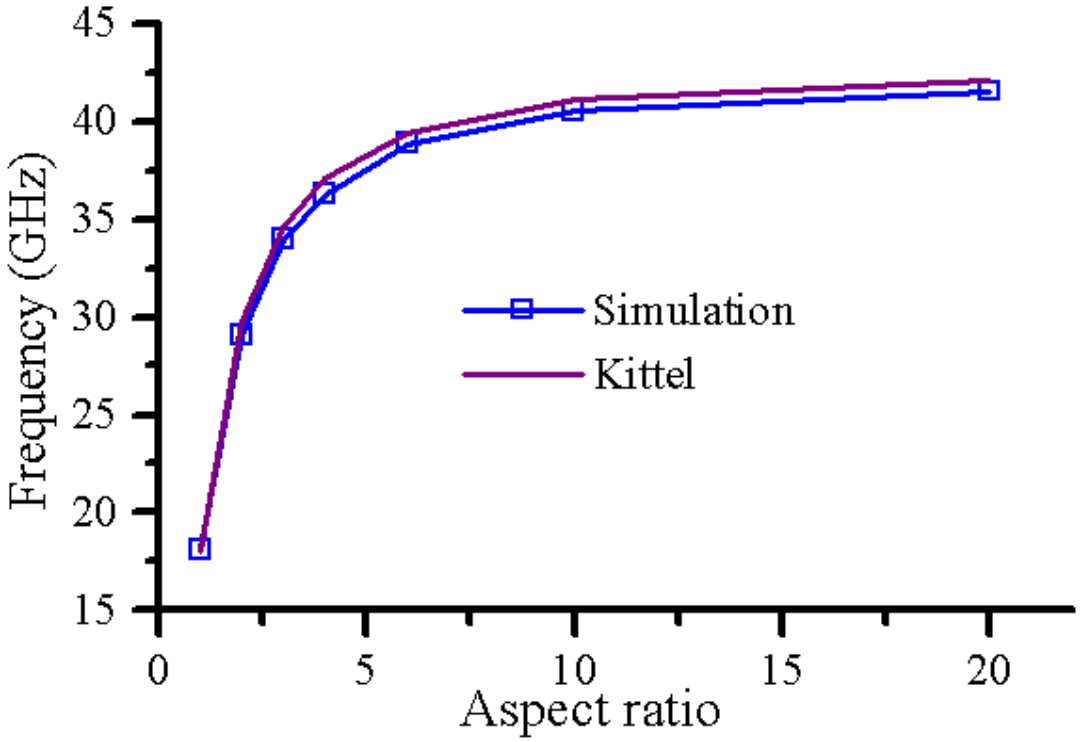

Figure 6
N. Dao, el al.